University of Zawia Journal of Engineering Sciences and Technology (UZJEST)
Volume 4, Issue 1, (2026), pp 51-63, ISSN 3006-2764

Thermal Analysis of 11 kV PILC Belted Cable

Mohamed Alsharif*[1], Khlid Ben Hamad[2], Abdulgader Alsharif[3]

[1] Department of Communication and Information Technology, Technical College of Civil Aviation and Meteorology, Espia, Libya

[2] Department of Electrical and Electronic Engineering, Faculty of Engineering Fezzan, University Fezzan, Libya

[3] Department of Electric and Electronic Engineering, College of Technical Sciences, Sebha, Libya

*Corresponding author email: moh.alsharif@sebhau.edu.ly

Received: 23-05-2026 | Accepted: 14-07-2026 | Available online: 20-07-2026 | DOI:10.26629/uzjest.2026.05

ABSTRACT

Worldwide, electrical networks depend on large Medium Voltage (MV) Paper Insulated Lead Covered (PILC) underground cables. Most of those cables were installed in past decades, with an expected lifespan of forty to seventy years. Today, most of these cables have exceeded their design service life, increasing the likelihood of MV network failures. In addition, during service, these cables are subjected to multiple stresses, including electrical, mechanical, and thermal stresses. The majority of their failures are attributed to thermal stress effects. The operational reliability of MV cables is influenced by thermal behaviour over time. This paper presents a comprehensive thermal model of a three-phase, belted 11 kV PILC cable system based on the Finite Element Method (FEM). Taking into account the ampacity, cable structure, installation layout, and the thermal characteristics of the soil under specific ambient conditions. Thermal behavior is investigated under constant load and cyclic daily loading. Power loss is determined and included in the thermal analysis. The thermal effect of each cable component is determined. The results demonstrated a significant time-varying temperature gradient within the cable. It indicates that the thermal characterization of PILC cables is highly sensitive to the operating load and that cable performance is significantly influenced by temperature variations over the cable layers. This research provides knowledge, modelling and analysis of underground MV PILC cable thermal behaviour. Leading to improved assessments and network lifespan extension.

Keywords: PILC MV cables, thermal performance, thermal modelling, time-varying loading, power losses.

التحليل الحراري لكابل شريطي بجهد 11 kV معزول بالورق المشبع بالزيت

محمد الشريف[1]، خالد بن حماد[2]، عبد القادر الشريف[3]

[1]قسم هندسة الاتصالات وتقنية معلومات الطيران، كلية تقنية الطيران المدني والأرصاد الجوية، اسبيعة، ليبيا

[2]قسم الهندسة الكهربائية والإلكترونية، كلية الهندسة، جامعة فزان، الرقيبة، ليبيا

[3]قسم الهندسة الكهربائية والإلكترونية، كلية العلوم التقنية، سبها، ليبيا

ملخـــــــص البحـــــــث

عالميًا، تعتمد الشبكات الكهربائية ذات الجهد المتوسط بشكل كبير على الكابلات الأرضية المعزولة بالورق المشبع بالزيت. وقد تم تركيب معظم هذه الكابلات خلال العقود الماضية، بعمر افتراضي يتراوح بين أربعين وسبعين عامًا. وقد تجاوزت معظم هذه الكابلات عمرها الافتراضي، مما يؤدي إلى حدوث أعطال متكررة ويرجع ذلك إلى التأثيرات الحرارية. تتناول هذه الورقة دراسة نموذج حراري لنظام كابل 11 كيلو فولت أرضي شريطي ثلاثي الطور معزول بالورق المشبع بالزيت، باستخدام طريقة العناصر المحدودة، مع الأخذ في الاعتبار سعة التيار الكهربائي ومكونات الكابل وطريقة تركيبه والبيئة المحيطة به ودرجة الحرارة المحيطة. تمت دراسة الاستجابة الحرارية للكابل تحت ظروف تشغيل بحمل ثابت وحمل يومي متغير، كما تم حساب الفواقد الحرارية للكابل، وتقييم التأثير الحراري لكل مكوّن من مكونات الكابل. أظهرت النتائج وجود تدرج حراري ملحوظ متغير مع الزمن داخل الكابل. كما بينت أن الخصائص الحرارية لكابلات الجهد المتوسط المعزولة بالورق المشبع بالزيت شديدة الحساسية لحمل التشغيل وأن أداء الكابل يتأثر بشكل كبير بتغيرات درجة الحرارة عبر مكوناته المختلفة. يقدم هذا البحث فهمًا حول النمذجة والطبيعة الحرارية لهذه الكابلات، إضافةً إلى منهجية لتقييمها وتحليل أدائها، مما يسهم في تحسين تقييماتها وإطالة العمر التشغيلي للشبكة الكهربائية.

الكلمات الدالة: كوابل الجهد المتوسط المعزولة بالورق المشبع بالزيت، الأداء الحراري، النمذجة الحرارية، الحمل اليومي المتغير مع الزمن، فواقد الطاقة الحرارية.

1. Introduction

In past decades, MV electrical distribution networks were mainly using PILC cables, and many of them still remain in service [1, 2]. Today, most of these cables have exceeded their design service life of forty to seventy years, increasing the probability of MV network failures [3]. The ageing of insulating materials affects the cable system, thereby reducing operational efficiency [4, 5]. Furthermore, ageing factors such as thermal, electrical, and mechanical stresses act on the cable system. The thermal stress is the primary factor that influences performance and accelerates cable degradation [6, 7]. Moreover, thermal stress due to the continuous change in temperature over time strains the cable insulation [8]. Also, increasing the temperature above the maximum standard rated conductor temperature of the cable may lead to cable degradation [9]. The maximum continuous operating conductor temperature of three-core belted PILC 11 kV cables is 65°C [10].

The conductor’s electrical resistance resists the flow of electric current. This produces heat in the conductor as Joule heating. The heat generated is directly proportional to the current load. It increases as the load increases and decreases as it decreases. High load magnitudes over load cycles lead to higher thermal stress within the insulating materials and vice versa [11, 12]. In addition, variations in load cycles during cable operation induce repeated thermal variations. This results in the expansion and contraction of the cable’s constituent materials. Furthermore, the temperature variations affect material dimensions by causing them to expand during heating and contract during cooling. The different thermal expansion coefficients of the constituent materials result in internal overstress during temperature variations. Also, the copper conductor exerts a force on the insulator that can exceed the strength of the material. This conductor behaviour weakens the dielectric material, which potentially accelerates insulation degradation [13, 14]. Moreover, the cable’s insulation structure across the vertical and horizontal planes becomes non-uniform as the insulation size changes. This leads to the degradation of the insulation [15, 16].

Temperature fluctuations significantly affect the viscosity and density of the impregnating compound within the paper insulation. High temperatures lead to a decrease in both the viscosity and density of the oil, causing volumetric expansion that raises the internal hydrostatic pressure and enhances oil mobility. This elevated pressure forces the fluid into regions of degraded or low-density insulation. During low-load conditions, the oil's viscosity and density increase as it cools, causing its volume to contract. In the cooling phase, this contraction results in a drop in internal pressure, which subsequently accelerates the degradation of the insulation's dielectric performance [17–19].

The majority of failures in medium-voltage underground PILC cables are attributed to thermal effects [1]. Medium-voltage PILC belted cables are particularly sensitive to temperature fluctuations induced by load current. In these systems, temperature acts as a primary driver of cable degradation [20, 21]. Thermal cycling is considered the main catalyst for dielectric exhaustion in PILC insulation. Over time, the insulation degrades which results in cable failure and potential interruption of the power supply [22]. The underground cable assessment during operation is critical for predicting their condition and preventing catastrophic faults. In addition, Monitoring the thermal condition of MV cables allows the detection of incipient insulation degradation. Real-time thermal assessment is essential for maintaining network reliability, reducing outages, and extending the service life of underground cable assets [23–25]. Although extensive research has been conducted on predicting the underground cable's thermal behaviour, a lack of practical knowledge continues to challenge utility operators [26–28]. Accurately predicting the thermal efficiency of underground cables under varying operational with environmental conditions remains difficult [29, 30]. Furthermore, real-time temperature measurement is often constrained by several factors, including soil thermal properties, load fluctuations, installation conditions (direct burial or ducts), cable depth and configuration, seasonal variations, insulation aging, and electromagnetic interference [11, 31]. As a result, accurately assessing cable temperature and optimizing ampacity during operation remain limited [24, 32]. The implementation and reliability of real-time temperature monitoring systems continue to represent significant challenges [26, 33, 34].

Power grids are expected to face increasing challenges in the future due to the extensive use of MV PILC cables and the rising failure rates [2]. A primary limitation related to the thermal characteristics of PILC cable dielectric [35]. The three-core PILC belted cables' thermal behavior is complex due to their multilayer insulation structure [36]. Also, environmental factors affect heat dissipation and temperature distribution within the cable layer which make accurate real-time temperature measurement challenging. Cable system parameters vary under different environmental conditions. Therefore, it is difficult to control the cable in real time [30]. The conductor temperature cannot be monitored during normal system operation [34]. Understanding cable thermal behavior is needed for accurate assessment and effective optimization of ampacity in real-time operation.

This paper investigates the thermal behavior of a belted medium-voltage paper-insulated lead-covered underground cable. The finite element method, implemented in COMSOL Multiphysics, is used to model a buried 11 kV three-core PILC cable. The thermal field response under varying load conditions is predicted. The thermal behavior, temperature characterization, and field distribution of the underground cable system are analyzed under different loading scenarios. The simulation results provide a detailed overview of the thermal variations within a typical PILC cable. Figure 1 illustrates the cable geometry under study [37]. The cable has a radius of 33.9 mm and a copper conductor size of 240 mm^2.

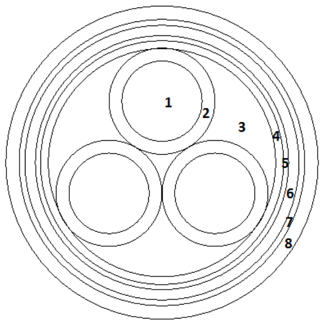

Figure 1: PILC cross section: copper conductor (1), oil-impregnated paper (2), filler (3), belt (4), lead sheath (5), bedding (6), armouring (7), and outer protective sheath (8) [37].

2. Methodology

2.1 Thermal Field Model

A thermal field model of PILC cable was developed to simulate its thermal response under steady-state and diurnal loading conditions. The simulations were carried out over one day. This duration captures the naturally varying thermal response of underground cable systems to ambient temperature variations [15]. The model first simulated a steady-state case at 100 A. It was then applied to a diurnal loading profile using time-series data from a real load over a 24-hour period [38]. A two-dimensional semicircular domain with a 6-meter diameter containing the cable within the trench fill and surrounding soil was established. The cable was laid at a depth of 0.3-meter within a 0.6 × 0.6-meters square sand trench filled, which was flush with the ground surface. This shallow burial depth was selected to evaluate the influence of dynamic surface boundary conditions, including solar irradiance and soil drying, on the cable's thermal performance. The primary source of ohmic heating in the cable system is Joule heating. The power loss (Ploss) results from the conductor's electrical resistance R, and the current magnitude square I^2, given by:

$$P_{loss} = I^2 R \quad (1)$$

The model calculates cable thermal behaviour in response to constant or diurnal loading inputs, based on specific environmental and installation settings. This behaviour is governed by the conservation of thermal energy in a dielectric material with respect to time, given by:

$$\frac{\partial T}{\partial t} \rho C_p + \nabla \cdot q = 0 \quad (2)$$

Where: T, temperature (K or °C). t, time (s). ρ, dielectric material density (kg/m³). C_p, specific heat capacity ($J \cdot kg^{-1} \cdot K^{-1}$). q, heat flux vector ($W \cdot m^{-2}$). $\nabla \cdot q$, heat flux divergence ($W \cdot m^{-3}$)

To solve Equation (2) as a heat transfer problem, Fourier's material law is introduced to link the heat flow with the thermal gradient:

$$q = -K\ (\nabla T) \quad (3)$$

Here, k= material thermal conductivity ($W.m^{-1} \cdot K^{-1}$).

By substituting equation (3) into equation (2) with the inclusion of a heat generation term Q, the heat conduction equation becomes:

$$\rho C_p \frac{\partial T}{\partial t} = K\, \nabla^2 T + Q \quad (4)$$

Given that the cable length is significantly greater than its diameter and that heat flows from the conductor through the insulation into the surrounding ground, axial heat flow is considered negligible relative to radial heat flow [9, 39]. As a result, heat flow is typically modelled as two-dimensional.

To solve the heat transfer problem in two dimensions, the heat diffusion equation (4) can be expressed using the Laplace operator as

$$\rho C_p \frac{\partial T}{\partial t} = K\left(\frac{\partial^2 T}{\partial x^2} + \frac{\partial^2 T}{\partial y^2}\right) + Q \tag{5}$$

Based on the specified thermal conductivity and internal heat generation, Equation (5) is used to calculate the temperature within the cable. It allows for analysis of the power cable's thermal circuit by incorporating the boundary conditions.

2.2 Boundary conditions:

The computational domain is defined by the topsoil and a deep semicircular perimeter that penetrates the present soil. The two boundaries are assigned specific thermal boundary conditions to represent the surrounding environment.

Thermal boundary conditions are imposed on the cable materials, including insulated boundaries at the surroundings and initial temperature conditions. The boundaries of the computational domain including the topsoil, the semicircular distance perimeter within the present soil, and the initial condition are defined at 288 K (15 °C) accordingly [40].

The interfaces between different cable materials and the boundaries are defined to maintain continuity of heat flow, expressed as

$$q_1 = q_2 \tag{6}$$

where $q_1$represents the incoming heat flux and $q_2$represents the outgoing heat flux.

The thermal conductivity values in ($W.m^{-1}\cdot K^{-1}$) are specified as follows: 0.833 for the native soil, 0.2 for the sand backfill and for the insulation material.

The cable was assumed to be buried in dry backfill to represent a conservative, worst-case scenario. During continuous operation, the heat generated by the cable induces moisture migration away from the conductor, which reduces the soil's thermal conductivity. This localized drying increases the thermal resistance of the sand backfill. It limits heat dissipation from the cable and results in higher operating temperatures. Therefore, the dry backfill assumption provides a conservative baseline for assessing the cable's thermal performance under the most adverse operating conditions.

2.3 Thermal Parameter Calculations

Two heat source terms are considered in the model: The ohmic losses result from the current flowing in the conductors (Q_c) and the heat generated by induced currents in the lead sheath (Q_s) and steel armour (Q_a), according to [41].

The core heat losses, Q_c, are given by:

$$Q_c = \frac{I^2 R}{A_c} \tag{7}$$

Where I is the conductor current, and R is the alternating current resistance, which is given as:

$$R = R_{dc}\,(1 + y_s + y_p) \tag{8}$$

Here, R_{dc} represents the conductor resistance at the maximum operating temperature, expressed as:

$$R_{dc} = \frac{R_{20}[1+\alpha_{20}(T-20)]}{A_c} \tag{9}$$

Here, the linear relationship is given by $[1 + \alpha_{20}(T - 20)]$. The resistance increases as temperature increases above 20°C and reduces as it falls below 20°C.

α_{20}, electrical resistivity temperature coefficient at 20°C, (1/K).

T is the operating conductor temperature (in °C).

R_{20} is the resistance in ohm/metre of a conductor at temperature 20°C is given below;

$$R_{20} = \frac{\rho_{20}}{A_c} \tag{10}$$

where ρ_{20} is the material electrical resistivity at 20°C, and A_c, conductor cross section, expressed as:

$$A_c = \frac{{d_c}^2\pi}{4} \tag{11}$$

where d_c is the conductor diameter

Proximity Effect Factor y_p:

The mutual inductance between conductors of adjacent phases. For a three-core cable, it is given by:

$$y_p = \frac{X_p^4}{192+0.8\cdot X_p^4}\left(\frac{d_c}{s}\right)^2\left[0.312\cdot\left(\frac{d_c}{s}\right)^2 + \frac{1.18}{\frac{X_p^4}{192+0.8\cdot X_p^4}+0.27}\right] \tag{12}$$

Here: s is the spacing among core axes, and X_p is an argument, which is given as:

$$X_p = \sqrt{\frac{(8\cdot\pi\cdot f\cdot k_p\cdot 10^{-7})}{R_{dc}}} \tag{13}$$

Where: f is the system frequency, 50 Hz.

k_p is the factor used in calculating the proximity effect.

The skin effect factor y_s:

Skin effect is a phenomenon where the effective conductor resistance increases due to self-inductance. It causes the core current density to increase toward the surface. y_s is given as:

$$y_s = \frac{x_s^4}{192+0.8\cdot x_s^4} \tag{14}$$

The dimensionless parameter x_s is obtained by:

$$x_s = \sqrt{\frac{4\cdot\omega\cdot k_s\cdot 10^{-7}}{R_{dc}}} \tag{15}$$

where k_s is the factor used in calculating the skin effect.

ω is the angular frequency in rad/s, expressed as:

$$\omega = 2\pi f \tag{16}$$

During cable operation, dielectric losses P_d arise as heat is stored in the insulation material. These losses are very small and are often neglected in practical analysis; however, they can be calculated using the equation below [42, 43, 1].

$$P_d = V^2 \cdot \omega \cdot C \cdot tan\delta \quad (17)$$

Where V is the voltage across the dielectric, C is the Cable capacitance per meter and $\tan\delta$ is the dielectric loss tangent.

The lead sheath heat losses Q_s are defined in terms of Q_c , using the equation:

$$Q_s = \lambda_s \frac{Q_c}{A_s} \quad (18)$$

Where the sheath cross section is given by:

$$A_S = \frac{((d_s)^2 - (d_i)^2)\pi}{4} \quad (19)$$

Where d_s is the diameter of the sheath, and $d_i$is the diameter of the cable insulation.

The sheath DC resistance, R_s is expressed as follows:

$$R_s = \frac{R_{20}[1+\alpha_{20}(T-20)]}{A_s} \quad (20)$$

The sheath Loss factor:

In a 3-core belted cable with a common sheath, the circulating currents cancel out and are negligible, and the sheath losses are primarily due to eddy currents, given by:

$$\lambda_s = \frac{3R_s}{R}\left[\left[\frac{2c}{d_s}\right]^2 \frac{1}{1+\left(\frac{R_s}{\omega}10^7\right)^2}\right] \quad (21)$$

The armour loss Q_a is defined in terms of Q_c , using the equation:

$$Q_a = \lambda_a \frac{Q_c}{A_a} \quad (22)$$

The armour cross section is given by:

$$A_a = \frac{((d_a)^2 - (d_b)^2)\pi}{4} \quad (23)$$

where d_a is the armour diameter, and d_b is the cable bedding diameter.

Loss factor in the armour is λ_a:

In 3-core cables, steel armour losses result from the magnetic field given by:

$$\lambda_a = 1.23\frac{R_a}{R}\left[\left[\frac{2c}{d_a}\right]^2 \frac{1}{1+\left(\frac{R_a}{\omega}10^7\right)^2}\right] \quad (24)$$

Where c is the spacing between a conductor axis and the cable axis

R_a is the armour resistance at actual temperature, which is given as:

$$R_a = \frac{R_{20}[1+\alpha_{20}(T-20)]}{A_a} \quad (25)$$

The heat transfer from the cable system into the surrounding environment is governed by the geometric configuration and the cable material properties [44]. Furthermore, the thermal dissipation is influenced by the thermal resistivity of the trench backfill and the prevailing environmental conditions.

To evaluate thermal heating stresses and cable structural variations within the system, the thermal swing parameters are defined:

Thermal Element Swing:

It represents the temperature range experienced by an individual cable component (ΔT). It is the temperature range between the maximum temperature T_{max} and minimum temperature T_{min} , experienced by the element, given as:

$$\Delta T = T_{max} - T_{min} \tag{26}$$

3. Results:

3.1 Results under Constant Load

The thermal three-core PILC belted cable response was predicted under constant load condition. The cable was subject to 100 A within 24-Hour duration. Figure 2 presents the thermal behavior results. It shows the temperature values at four locations. The blue curve represents the conductor core temperature, green curve represents the lead sheath temperature, red curve represents the armour, and cyan represents the temperature of the outer sheath. The response curves exhibit fast and slow components. The cores exhibit the fastest heating whereas the lead sheath exhibits lower heating than the cores. The armour heating remains lower than that of the lead sheath and the outer sheath exhibits the lowest heating. In addition, the components close to the core exhibit fast heating due to the effect of the main heat source. The further components from the core exhibit less heating due to the effect of the trench-fill material surrounding the cable.

The figure 2 also shows a constant temperature variation between different cable components. It is 1.3 K between the cores and the lead sheath, 1.2 K between the lead sheath and the armour, 2.1 K between the armour and the outer sheath, and 4.6 K between the cores and the outer sheath. The constant temperature variations between the cable elements are based on the fact that the cable elements are made of different materials. Therefore, each component has its own constant thermal resistance which affects the temperature rise among the cable elements.

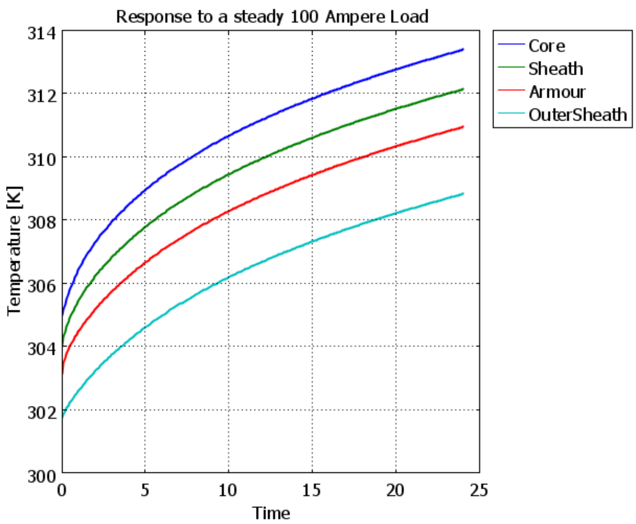

Figure 2: Thermal profile of the installed belted PILC cable showing the temperature evolution at four layers: the conductor core (blue), the lead sheath (green), the armour (red) and the outer sheath (cyan).

3.2 Diurnal Thermal Response Results

The thermal behaviour of the three-core PILC belted cable was predicted under diurnal loading conditions. The simulation was run for a 24-Hour duration based on measured real load input data [37]. The cable operating temperature changes based on daily loading variations. The daily variation in load produces a variation in the cable operating temperature of a maximum of 12.3 K. The maximum temperature observed in the cable was 306.4 K at the conductor at 20:00, while the minimum temperature was 294.1 K at the outer sheath at 6:00. The temperature between the cable elements changes with time: The swing of the conductor and the lead sheath is 0.2 and 1.2 K; the swing of the lead sheath and the armour is 0.3 and 1.1 K; the swing of the armour and the outer sheath is 0.5 and 1.9 K; and the swing of the conductor and the outer sheath is 1 and 4.2 K. These temperature variations can be explained by the different thermal characteristics of the cable component materials, which result in different thermal manner. In addition, the variation in load causes temperature differences among the cable materials, resulting in different thermal responses. The thermal response of the core, sheath, armouring and jacket over one day due to the current load is illustrated in Figure 3. These results show the relationship between the daily loading and cable temperature and are in agreement with similar work [15, 44]. The input current load data for the cable model over one day are presented in Figure 4.

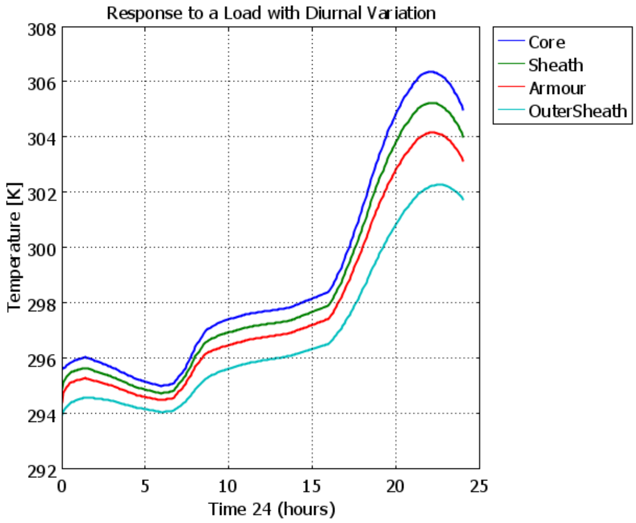

Figure 3: Thermal variation across the core, sheath, armouring and jacket during a day loading cycle.

Figure 4 shows the real current load used as input to the cable model over a 24-h period.

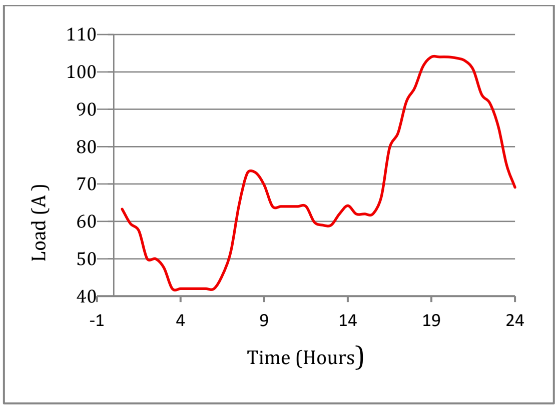

Figure 4: An Input current load data for the PILC cable model over a 24-h period [37].

Figure 5 shows the temperature gradient within the PILC cable at the peak temperature of 22:00 hour. The temperature is high in and around the conductors, and less far away. The temperature gradually decreases from the cable core of 306.4 K to an environmental soil temperature of 288.15 K. The temperature on the surface of the conductor remains uniform distribution within high value. This is due to the superior thermal conductivity of copper and the uniform distribution of ohmic heat. The temperature decreases gradually with distance from the cores. This is due to the increasing distance from the heat source. It is also due to the low thermal conductivity and high thermal resistance of the dielectric material and the surrounding environment.

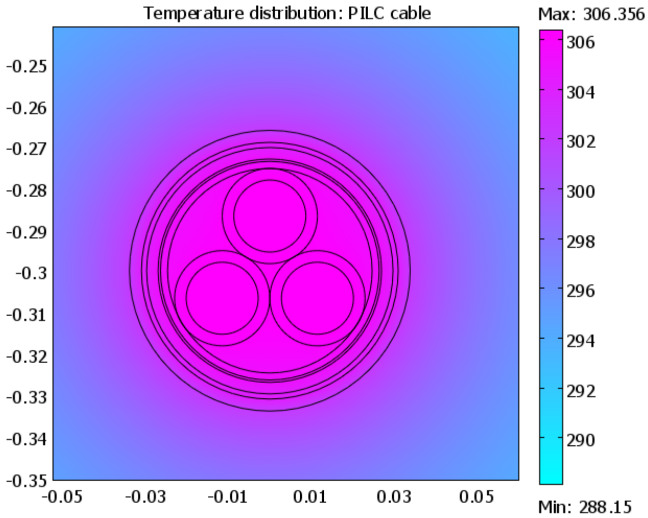

Figure 5: Cross-sectional temperature variation in the burial PILC cable.

Figure 6 illustrates the thermal field lines of the buried three-core PILC cable. Temperature lines are close to each other near the cores and spread farther apart away from them. In addition, the thermal field lines are close to each other where the loss is high and vice versa. A triangular heat distribution pattern is observed inside the cable. This indicates the hottest region of the insulation caused by the heat source.

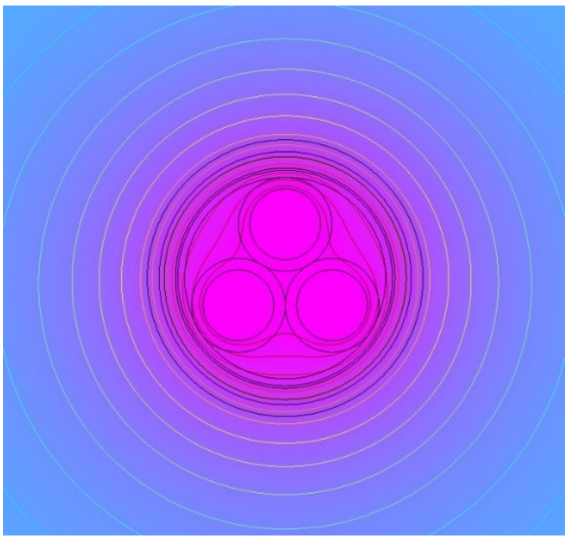

Figure 6: Thermal field of the buried three-core PILC cable under diurnal loading variation.

4. Conclusion

A comprehensive thermal model of a three-phase, belted 11 kV PILC underground cable system was modelled using the FAM. The thermal behaviour of a buried PILC belted cable with constant and diurnal loading conditions was analysed throughout a 24-H duration. Detailed thermal variations within a typical 11 kV PILC belted cable components are determined. The cable operated under realistic loading conditions show a significant periodic variation in the temperature. A significant time-varying temperature gradient was demonstrated within the cable. The thermal effect of each cable component has been calculated. The thermal characteristics of PILC cable materials are highly sensitive to the operating load. The variation in cable current load affects the temperature distribution of the cable components. A methodology that assesses MV PILC cables under loading variations is presented.

5. Limitations and Future Work

A limitation of this study is that the findings are based on finite element numerical simulations. Future work will focus on experimental validation using a physical cable setup under real-world operating conditions.

REFERENCES

[1] M. Zapf, T. Blenk, A. C. Müller, H. Pengg, I. Mladenovic, and C. Weindl, “Lifetime assessment of PILC cables with regard to thermal aging based on a medium voltage distribution network benchmark and representative load scenarios in the course of the expansion of distributed energy resources,” *Energies*, vol. 14, no. 2, p. 494, 2021, doi: 10.3390/en14020494.

[2] A. Rafati, H. Mirshekali, H. R. Shaker, and N. Bayati, “Power grid renovation: A comprehensive review of technical challenges and innovations for medium voltage cable replacement,” *Smart Cities*, vol. 7, no. 6, pp. 3727–3763, 2024, doi: 10.3390/smartcities7060146.

[3] M. A. Alsharif, P. A. Wallace, D. M. Hepburn, and C. Zhou, “Electric field investigation in MV PILC cables with void defect,” *International Journal of Electrical, Computer, Electronics and Communication Engineering*, vol. 9, no. 1, 2015, doi: 10.5281/zenodo.1098853.

[4] G. V. Bezprozvannych, Y. S. Moskvitin, I. O. Kostiukov, and O. M. Grechko, “Dielectric parameters of phase and belt paper impregnated insulation of power cables,” 2025, doi: 10.1109/ukrcon60879.2025.10512345.

[5] I. Mladenovic and C. Weindl, “Dependencies of the PD- and tan (δ)-characteristics on the temperature and ageing status of MV PILC cables,” in *Proc. 2011 Electrical Insulation Conf. (EIC)*, Jun. 2011, pp. 88–92, doi: 10.1109/EIC.2011.5995083.

[6] A. C. Domingos, L. Duarte, A. P. Pinheiro, F. A. M. Moura, L. Vasconcelos, D. P. de Carvalho, F. E. d. F. Fadel, and P. N. Sakai, “Comparative analysis of insulation aging in cross-linked polyethylene and ethylene–propylene rubber cables through the progression rate of partial discharge,” *Energies*, vol. 18, no. 10, p. 2653, 2025, doi: 10.3390/en18102653.

[7] M. Alsharif, P. A. Wallace, D. M. Hepburn, and C. Zhou, “Partial discharge resulting from internal degradation in underground MV cables: Modelling and analysis,” in *Proc. 44th Int. Universities Power Engineering Conf. (UPEC)*, Sep. 2009, pp. 1–5, doi: 10.1109/UPEC.2009.5429440.

[8] Q. Shao, S. Fan, Z. Zhang, F. Liu, Z. Fu, P. Lv, and Z. Mu, “Artificial intelligence in cable fault detection and localization: Recent advances and research challenges,” *Energies*, vol. 18, no. 14, p. 3662, 2025, doi: 10.3390/en18143662.

[9] Q. M. Hoang, H. D. Tran, and N. T. T. Vu, “A simulation method for temperature monitoring of medium voltage underground cables insulation,” *Int. J. Electr. Electron. Eng. & Telecomms.*, vol. 14, no. 3, pp. 180–187, 2025, doi: 10.18178/ijeetc.14.3.180-187.

[10] British Standards Institution, *BS 6480:1988: Specification for impregnated paper-insulated lead or lead alloy sheathed electric cables of rated voltages up to and including 33 000 V*, London, U.K.: BSI, 1988. ISBN-10: 0580161056

[11] A. Sturchio, G. Fioriti, V. Salusest, L. Calcara, and M. Pompili, “Thermal behavior of distribution MV underground cables,” in *Proc. 2015 AEIT Int. Annual Conf. (AEIT)*, Naples, Italy, Oct. 2015, pp. 1–5, doi: 10.1109/AEIT.2015.7415247

[12] L. Calcara, S. Sangiovanni, and M. Pompili, “MV underground cables: Effects of soil thermal resistivity on anomalous working temperatures,” in *Proc. 2017 AEIT Int. Annual Conf. (AEIT)*, Cagliari, Italy, Sep. 2017, pp. 1–5, doi: 10.23919/AEIT.2017.8240508.

[13] R. Bartnikas and K. Srivastava, *Power and Communication Cables: Theory and Applications*, 1st ed. New York, NY, USA: Wiley-IEEE Press, 2003. ISBN: 978-0471452709.
[14] F. Aras, V. Alekperov, N. Can, and H. Kirkici, "Aging of 154 kV underground power cable insulation under combined thermal and electrical stresses," *IEEE Electr. Insul. Mag.*, vol. 23, no. 5, pp. 25–33, 2007, doi: 10.1109/MEI.2007.4318272.
[15] M. A. Alsharif, K. B. Hamad, A. Alsharif, and M. Salem, "Thermal analysis of medium voltage single core armoured XLPE cable," *African Journal of Advanced Pure and Applied Sciences*, vol. 5, no. 1, pp. 205–212, Feb. 2026. https://aaasjournals.com/index.php/ajapas/article/view/1851.
[16] A. M. Elsaid, M. S. Zahran, S. A. Abdel Moneim, A. Lasheen, and I. G. Mohamed, "A recent review on ventilation and cooling of underground high-voltage cable tunnels," *J. Thermal Anal. Calorimetry*, vol. 149, no. 17, pp. 8927–8978, 2024, doi: 10.1007/s10973-024-13299-x.
[17] P. Hyvönen, *Prediction of insulation degradation of distribution power cables based on chemical analysis and electrical measurements*, Doctoral dissertation, Helsinki University of Technology, Espoo, Finland, 2008, ISBN: 978-951-22-9402-2.
[18] C. Smith and M. Michel, "Influence of network events on partial discharge activity and cable health," in *Proc. 20th Int. Conf. on Electricity Distribution (CIRED)*, Prague, Czech Republic, Jun. 8–11, 2009, pp. 1–4, doi: 10.1049/CP.2009.0785.
[19] C. Ahmed and N. Srinivas, "Can the operating conditions of the cable system affect the data of the field PD testing?" in *Proc. 2001 Annual Report Conf. on Electrical Insulation and Dielectric Phenomena*, Kitchener, ON, Canada, Oct. 14–17, 2001, pp. 311–314, doi: 10.1049/cp:19990898.
[20] Y. Li and P. Wouters, "Implementation of temperature monitoring for MV cables based on signal propagation," in *Proc. 2022 IEEE International Conference on High Voltage Engineering and Applications (ICHVE)*, Chongqing, China, 2022, pp. 1–4, doi: 10.1109/ICHVE53725.2022.9961552.
[21] G. V. Bezprozvannych and Y. S. Moskvitin, "Physical processes of aging and assessment of the technical condition of power cables with paper-impregnated insulation," in *Proc. 2023 IEEE 4th KhPI Week on Advanced Technology (KhPIWeek)*, Kharkiv, Ukraine, Oct. 2–6, 2023, pp. 1–5, doi: 10.1109/KhPIWeek61412.2023.10312975.
[22] C. Weindl, I. Mladenovic, T. Scharrer, and R. Patsch, "Development of the p-factor in an accelerated ageing experiment of the MV PILC cables," in *Proc. 2010 10th IEEE Int. Conf. on Solid Dielectrics (ICSD)*, Jeju Island, South Korea, Jul. 2010, pp. 1–4, doi: 10.1109/ICSD.2010.5594815.
[23] P. A. Wallace, M. Alsharif, D. M. Hepburn, and C. Zhou, "Failure modes of underground MV cables: Electrical and thermal modelling," *Excerpt from the Proceedings of the COMSOL Conference 2009*, Milan, Italy, 2009. https://www.comsol.com/paper/failure-modes-of-underground-mv-cables-electrical-and-thermal-modelling-6783.
[24] Y. Zhang, F. Yu, Z. Ma, J. Li, J. Qian, X. Liang, and M. Zhang, "Conductor temperature monitoring of high voltage cables based on electromagnetic-thermal coupling temperature analysis," *Energies*, vol. 15, no. 2, p. 525, 2022, doi: 10.3390/en15020525.
[25] H. Zhao, Z. Zhang, Y. Yang, J. Xiao, and J. Chen, "A dynamic monitoring method of temperature distribution for cable joints based on thermal knowledge and conditional generative adversarial network," *IEEE Trans. Instrum. Meas.*, vol. 72, pp. 1–14, 2023**,** doi: 10.1109/TIM.2023.3289014.
[26] S. Ahmad, Z. H. Rizvi, and F. Wuttke, "Unveiling soil thermal behavior under ultra-high voltage power cable operations," *Scientific Reports*, vol. 15, no. 1, p. 7315, 2025, doi: 10.1038/s41598-025-91831-1.
[27] M. M. Matshoge, B. Mendu, B. B. Monchusi, and S. Mbuyu, "Power Cable Insulation Degradation, Fault Detection, and Lifetime Modelling: A Systematic Review of Advanced Analytical and Machine Learning Approaches," in *Proc. 2025 5th Int. Conf. on Electrical, Computer, Communications and Mechatronics Engineering (ICECCME)*, Oct. 2025, pp. 1–10, doi: 10.1109/ICECCME64568.2025.11277787.
[28] Y. Li, L. Jiang, M. Xie, J. Yu, L. Qian, K. Xu, M. Chen, and Y. Wang, "Advancements and challenges in power cable laying," *Energies*, vol. 17, no. 12, p. 2905, 2024, doi: 10.3390/en17122905.
[29] P. Navarrete-Rajadel, P. Llovera-Segovia, V. Fuster-Roig, and A. Quijano-López, "A sensor for multi-point temperature monitoring in underground power cables," *Sensors*, vol. 25, no. 17, p. 5490, 2025, doi: 10.3390/s25175490.
[30] X. Chen, H. Wang, H. Zhang, Z. Zhang, S. Li, K. Liu, and Z. Ma, "A digital twin model of the axial temperature field of a DC cable for millisecond calculations," *Electric Power Syst. Res.*, vol. 233, p. 110460, 2024, doi: 10.1016/j.epsr.2024.110460.
[31] P. A. A. F. Wouters, P. C. J. M. van der Wielen, B. Kruizinga, and P. Wagenaars, "Challenges in wave-velocity based cable temperature monitoring for widespread implementation in medium-voltage networks," in *Proc. 2024 IEEE Int. Conf. on High Voltage Engineering and Applications (ICHVE)*, Berlin, Germany, 2024, pp. 1–4, doi: 10.1109/ICHVE61955.2024.10676078.
[32] B. A. Atoccsa, D. W. Puma, D. Mendoza, E. Urday, C. Ronceros, and M. T. Palma, "Optimization of ampacity in high-voltage underground cables with thermal backfill using dynamic PSO and adaptive

strategies," *Energies*, vol. 17, no. 5, p. 1023, 2024, doi: 10.3390/en17051023.
[33] H. Zhao, Z. Zhang, Y. Yang, P. Gan, and X. Liu, "Real-time reconstruction of temperature field for cable joints based on inverse analysis," *Int. J. Electr. Power Energy Syst.*, vol. 144, p. 108573, 2023, doi: 10.1016/j.ijepes.2022.108573.
[34] M. Lin, Q. Shi, and T. Wang, "Temperature and humidity sensor monitoring of directly buried cable based on temperature field distribution simulation of power cable," *J. Meas. Eng.*, vol. 11, no. 2, pp. 154–165, Jun. 2023, doi: 10.21595/jme.2023.23178.
[35] Y. Li, P. A. A. F. Wouters, P. Wagenaars, P. C. J. M. van der Wielen, and E. F. Steennis, "Temperature dependent signal propagation velocity: possible indicator for MV cable dynamic rating," *IEEE Trans. Dielectr. Electr. Insul.*, vol. 22, no. 2, pp. 665–672, Apr. 2015, doi: 10.1080/15583724.2015.1044228.
[36] C. Zhou, H. Yi, and X. Dong, "Review of recent research towards power cable life cycle management," *IET High Voltage*, vol. 2, no. 3, pp. 179–187, 2017, doi: 10.1049/hve.2017.0037.
[37] M. A. Alsharif and I. S. Naser, "Partial discharge activity in PILC belted medium voltage cable," *J. Pure Appl. Sci. (JOPAS)*, vol. 6, no. 1, pp. 2521-9200, Oct. 2020. doi:10.51984/jopas.v19i5.779.
[38] D. M. Hepburn, C. Zhou, X. Song, G. Zhang, and M. Michel, "Analysis of online power cable signals," in *Proc. International Conference on Condition Monitoring and Diagnosis*, Beijing, China, Apr. 21–24, 2008, pp. 1175–1178, doi: 10.1109/CMD.2008.4580497.
[39] G. J. Anders, *Rating of Electric Power Cables in Unfavorable Thermal Environment*, Hoboken, NJ, USA: John Wiley & Sons, 2005, ISBN: 978-0471723837.
[40] IEC 60287-3-1:1995, *Electric cables—Calculation of current rating—Part 3: Sections on operating conditions*, Geneva, Switzerland: International Electrotechnical Commission, 1995. https://www.iec.ch/standards.
[41] BS IEC 60287-1-1:2006, *Electric cables—Calculation of current rating—Part 1-1: Current rating equations (100% loss factor) and calculation of losses general*, London, U.K.: British Standards Institution, 2006. knowledge.bsigroup.com
[42] F. Aras and Y. Biçen, "Thermal modelling and analysis of high-voltage insulated power cables under transient loads," *Comput. Appl. Eng. Educ.*, vol. 21, no. 3, pp. 516–529, 2013, doi: 10.1002/cae.20497.
[43] M. A. Camalov, A. O. Orucov, H. S. Aliyev, and E. F. Bagirli, "Assessing dielectric property variations in XLPE insulated composite materials under different voltage and frequency," in *Proc. VI Int. Sci. Pract. Conf. "Energy- and Resource-Saving Technologies: Experience and Perspectives"*, Kyzylorda, Kazakhstan, 2024, pp. 119–129. www.researchgate.net.
[44] P. A. Wallace, D. M. Hepburn, C. Zhou, and M. Alsharif, "Thermal response of a three-core belted PILC cable under varying load conditions," in *Proc. 20th Int. Conf. and Exhibition on Electricity Distribution – Part 1 (CIRED)*, Jun. 2009, pp. 1–4, doi: 10.1049/cp.2009.0801